Theory and Practice of Science and Technology
2025, VOL. 6, NO. 12, 61-66
DOI: 10.47297/taposatWSP2633-456913.20250612

Intelligent Dynamic Modeling and Adaptive Optimization for Non-Invasive Microwave Hyperthermia Systems

Mengqing Sun

University of Shanghai for Science and Technology, Shanghai, 200093, China

ABSTRACT
Microwave hyperthermia is an emerging non-invasive therapeutic modality for cancer treatment that relies on controlled heating of tumor tissue. Accurate prediction of internal temperature is critical to ensure therapeutic efficacy while avoiding damage to surrounding healthy tissues. This paper proposes a hybrid system identification framework that integrates the Sooty Tern Optimization Algorithm (STOA) with a Forgetting Factor Recursive Least Squares (FFRLS) algorithm to estimate the internal temperature of microwave-heated tissues based on surface temperature measurements. A linear-in-parameters model is developed to capture the dynamic thermal behavior of tissue heating and heat conduction. The STOA is employed to perform global exploration of the parameter space and effectively mitigate premature convergence to local optima, while the FFRLS algorithm provides online refinement and real-time adaptive updating of model parameters. Experimental results demonstrate that the proposed STOA-FFRLS method significantly outperforms the conventional RLS approach in terms of estimation accuracy and numerical stability, yielding substantially reduced modeling errors and residual fluctuations. The validated model facilitates the development of a non-invasive, high-precision thermal monitoring framework for safe and effective microwave hyperthermia treatment.

KEYWORDS
Microwave hyperthermia; Rls; Stoa; System identification; Data-driven modeling

1 Introduction

Microwave hyperthermia has emerged as a clinically valuable non-invasive modality for cancer treatment, leveraging focused electromagnetic energy to selectively elevate tumor temperatures to the therapeutic range of 42℃ to 45℃ and maintain it for a specific duration. By exploiting the difference in heat tolerance between tumor cells and normal tissues, this method enables selective cytotoxicity, thereby promoting the apoptosis of cancer cells. Previous studies have demonstrated its significant therapeutic efficacy, particularly in the treatment of breast cancer (2017)[1], and brain tumors (2025)[2]. The technique achieves precise heating of tumor tissues by efficiently transferring microwave energy, generated externally, to the targeted lesion within the body, a process influenced by the dielectric properties of tissues characterized in (2024) [3]. Currently, research in this field spans multiple domains, including superficial hyperthermia (2024) [4], deep tissue hyperthermia, and whole-body microwave hyperthermia (2024)[5], and non-invasive field shaping approaches.

However, a critical challenge in clinical application lies in the accurate measurement and control of the temperature at the heating site. Insufficient heating fails to achieve therapeutic efficacy, whereas excessive temperatures, while capable of eradicating tumor cells, may cause irreversible thermal damage to surrounding healthy tissues. For instance, simulations and experiments have shown that skin temperatures can rise to 60℃during breast cancer hyperthermia, highlighting the need for precise regulation. Moreover, when temperature sensors are implanted near the heated region, their readings can be significantly distorted due to microwave radiation interference, though non-invasive alternatives like the radio-thermal monitoring concept (2022) [6], address this issue with minimal electromagnetic interference. Non-invasive solutions, such as the Radio-Thermal Monitoring Sheet (R-TMS), enable real-time skin temperature sensing with reduced susceptibility to electromagnetic interference. Moreover, thermal-induced changes in tissue mechanics (2012)[7], further complicate the control problem and demand adaptive modeling strategies.

Although non-invasive techniques such as magnetic resonance thermometry (MRT) and ultrasound-based methods have been explored, they often fall short in real-time feedback capabilities due to equipment bulkiness, high cost, and limited temporal resolution. As a result, the development of non-invasive temperature measurement techniques has become a focal point of current research, the optimization of antenna excitations using particle swarm optimization (PSO) for 3D thermal focusing (2017) [1], which suffers from high computational cost due to the need for multi-parameter optimization with coupled electromagnetic – thermal simulations(2025) [8], and lacks adaptability to dynamic changes in tissue dielectric properties during treatment.

Offline field shaping methods, such as the angular spectrum projection approach, rely on oversimplified layered models and static tissue parameters, lacking mutual coupling compensation and real-time adaptability, which limits their accuracy in dynamic clinical scenarios, and differential evolution-based beamforming, allow high-precision control but depend on precomputed parameters and lack real-time adaptability. While dielectric property characterization of tissues, supports model accuracy, it is typically performed offline and cannot account for dynamic physiological variations during

treatment.

To address the limitations of offline models, online modeling techniques have been introduced. Lestini et al () [5] developed a wireless R-TMS system for superficial skin temperature monitoring during hyperthermia; however, the approach remains limited by its lack of dynamic modeling, failing to capture transient deep tissue temperature changes and thermal responses during treatment.

In recent years, swarm intelligence optimization algorithms have been widely used in solving complex problems due to their characteristics such as simple structure and easy implementation. The more popular algorithms include Genetic Algorithm (GA), Particle Swarm Optimization (PSO) algorithm, and Differential Evolution (DE) Algorithm, artificial Ant Colony Optimization (ACO), and Fruit Fly optimization algorithm (FOA), etc. Among these, STOA has gained prominence for its effective global exploration, balanced exploration-exploitation mechanism, and straightforward implementation. It has been applied across diverse domains including UAV path planning, futures market forecasting, power system optimization, process control, and supply chain management.

To bridge this research gap, this study develops a unified discrete-time Extended Auto-Regressive (ARX) model for microwave-heated biological tissues, formulated solely based on microwave input power and measured surface temperature data to streamline the modeling pipeline. Subsequently, a hybrid online identification scheme integrating the Sooty Tern Optimization Algorithm and Forgetting Factor Recursive Least Squares (STOA-FFRLS) is proposed to characterize the dynamic thermal conduction behaviors and nonlinear properties of tissues. By incorporating a weighting adjustment mechanism based on the instantaneous squared prediction error of residuals, the hybrid framework enables real-time parameter updating. In this framework, STOA facilitates global exploration of the parameter space through cooperative adaptive flight and spiral dive strategies, effectively mitigating local optima entrapment, while FFRLS continuously refines parameter estimates, thereby reducing the impact of measurement noise, modeling uncertainties, and the time-varying characteristics of thermal dynamics.

2 Establishment of the System Model

This section introduces a hybrid modeling framework dedicated to noninvasive temperature estimation for focused microwave hyperthermia procedures. The core objective is to infer the internal temperature at target regions (e.g., tumor lesions) exclusively on the basis of infrared thermography data acquired from the skin surface. Microwave energy is transmitted to deep-seated tissues, inducing a outward heat propagation process that ultimately reaches the body's surface.

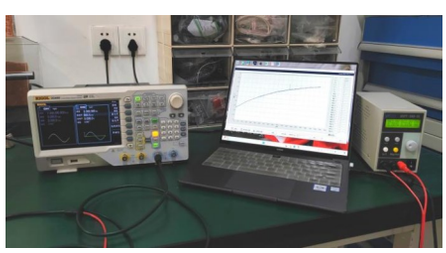

Figure 1 Experimental operation diagram

As illustrated in Figure 1, focused microwave energy heats the internal tissue, and the generated heat is conducted outward to the skin surface. By establishing a model that captures the relationship between internal and surface temperatures, the internal temperature can be inferred from the surface measurements. This modeling framework consists of two subsystems: (1) the internal heating dynamics governed by microwave absorption, and (2) the thermal conduction from the heating point to the surface.

2.1 Heating Model of Human Tissue

The first subsystem models the temperature evolution T_i within the tissue under microwave stimulation. The bioheat transfer equation is simplified by retaining the dominant terms:

$$\alpha C_t \frac{\partial T_i}{\partial t} = \gamma \nabla^2 T_i + \varphi P(u) \# \tag{1}$$

where, α is tissue density, C_t is the specific heat, γ denotes thermal conductivity, and $\nabla^2 T_i$ represents radial diffusion. The function $P(u) \propto u^2$ denotes microwave power deposition, scaled by a factor φ representing tissue absorption characteristics.

2.2 Temperature Conduction Model of Human Tissue

The second subsystem captures the conduction of heat from the internal site to the skin surface. A lumped-parameter first-order model relates the internal temperature T_i to the observed surface temperature T_o:

$$RC\frac{\partial T_o}{\partial t}+T_o=T_i+RQ_o\# \tag{2}$$

In thermally stable environments, ambient loss Q_o is negligible, simplifying the model to:

$$RC\frac{\partial T_o}{\partial t}+T_o=T_i\# \tag{3}$$

2.3 Unified Data-Driven Modeling Framework

Both subsystems are abstracted into a unified discrete-time ARX model, facilitating a data-driven approach to real-time estimation and prediction. The general model is:

$$\Phi\left(z^{-1}\right)\hat{T}_x(k)=\theta\left(z^{-1}\right)U(k)+\eta(k)\# \tag{4}$$

where, $\hat{T}_x(k)$ is the estimated output, $\theta\left(z^{-1}\right)$ models the input-output response and $\eta(k)$ is zero-mean Gaussian modeling noise. Equivalently, the model can be written in its canonical difference equation form:

$$y_k+a_1y_{k-1}+\cdots+a_ny_{k-n}=b_1u_{k-1}+\cdots+b_mu_{k-m}\# \tag{5}$$

where, y_k denotes the measured output, and u_k the system input; the coefficients $\{a_i\}$ and $\{b_i\}$form the parameter vector θ.

A regressor vector $\phi(k)$ is formulated on the basis of historical input-output datasets, with the corresponding model parameters θ being derived through offline estimation. For the heating model, this parameter identification task is accomplished by means of the GWO-FFRLS hybrid algorithm, which synergistically integrates the adaptive merits of recursive estimation with the global optimization capability inherent in evolutionary search strategies. In the case of the conduction model, a Newtonian iterative algorithm is implemented; herein, each descent step is calibrated via golden section search to guarantee a globally optimal reduction in predictive residuals. Upon completion of the identification process, the unified ARX model facilitates high-efficiency real-time temperature estimation and predictive control operations under both heating and conduction modalities.

3 STOA Identification Algorithm

The STOA is a bio-inspired optimization algorithm proposed by G. Dhiman and A. Kaur (2019) [9]. Inspired by the foraging behaviors of seabirds, this algorithm features strong global search capability and high precision. It mainly consists of two core phases: migration behavior (global exploration) and attack behavior (local exploitation).

3.1 Migration Behavior

Migration behavior (the exploration phase) consists of three core components: collision avoidance, aggregation, and position update. It guides the position update of other sooty terns by updating the position of the current optimal sooty tern.

3.1.1 Collision Avoidance

This step generates distinct positions via an additional variable to prevent collisions among sooty terns during migration. The calculation formula is:

$$\boldsymbol{C}_{st}=\boldsymbol{S}_A\times\boldsymbol{X}_{st}(\boldsymbol{z})\# \tag{6}$$

where, $\boldsymbol{C}_{st}$ denotes the collision-free position of the sooty tern individual, $\boldsymbol{X}_{st}$ is the current position of the sooty tern, $\boldsymbol{z}$ represents the current iteration number, $\boldsymbol{S}_A$ is a collision-avoidance variable factor used to compute the collision-free position, with the constraint:

$$\boldsymbol{S}_A=\boldsymbol{C}_f\left(1-\frac{\boldsymbol{Z}}{\boldsymbol{Z}_{max}}\right)\# \tag{7}$$

Where, $\boldsymbol{C}_f$ is a control variable for adjusting $\boldsymbol{S}_A$, $\boldsymbol{Z}_{max}$ is the maximum number of iterations. Typically, $\boldsymbol{C}_f$ is set to 2, so $\boldsymbol{S}_A$ linearly decreases from 2 to 0.

3.1.2 Aggregation

After collision avoidance, all sooty terns converge toward the optimal individual. Its mathematical expression is:

$$M_{St} = C_B \times \left(X_{bst}(z) - X_{st}(z) \right) \#(8)$$

Where, M_{St} describes the movement process of X_{st} (at different positions) toward the optimal position X_{bst}, C_B is a random variable that balances exploration and exploitation, calculated as

$$C_B = 0.5 \times R_{and} \#(9)$$

In the formula, R_{and} is a random number ranging from 0 to 1.

3.1.3 Position Update

Each sooty tern individual updates its position using the collision-free position $\boldsymbol{C_{st}}$ (from Eq. (1)) and the movement process $\boldsymbol{M_{St}}$ (from Eq. (3)), with the expression:

$$\boldsymbol{D_{st}} = \boldsymbol{C_{st}} + \boldsymbol{M_{st}} \#(10)$$

Where, $\boldsymbol{D_{st}}$ represents the distance between the current position and the optimal position.

3.2 Attack Behavior

During migration, sooty terns increase their flight altitude via wing adjustments, while continuously modifying their speed and flight angle to attack prey. Their circling behavior in the air can be defined as

$$\boldsymbol{x'} = \boldsymbol{R_{adius}} \times \mathbf{sin}\ \boldsymbol{i} \#(11)$$

$$\boldsymbol{y'} = \boldsymbol{R_{adius}} \times \mathbf{cos}\ \boldsymbol{i} \#(12)$$

$$\boldsymbol{z'} = \boldsymbol{R_{adius}} \times \boldsymbol{i} \#(13)$$

$$\boldsymbol{R_{adius}} = \boldsymbol{u} \times \boldsymbol{e^{kv}} \#(14)$$

In the formula, $\boldsymbol{x'}$, $\boldsymbol{y'}$ and $\boldsymbol{z'}$ are the three components of the spatial coordinate system, $\boldsymbol{R_{adius}}$ is the radius of each spiral, $\boldsymbol{i}$ is a variable in the set $[0,\ 2\boldsymbol{\pi}]$, $\boldsymbol{u}$ and are the constants defining the shape of the spiral, usually taken as 1, $\boldsymbol{e}$ is the base of the natural logarithm, $\boldsymbol{k}$ is the proportionality constant. The calculation formula for the new position after attacking the prey is

$$\boldsymbol{X_{St}}(\boldsymbol{z}) = \boldsymbol{D_{st}} \times \left(\boldsymbol{x'} + \boldsymbol{y'} + \boldsymbol{Z'} \right) \times \boldsymbol{X_{bst}}(\boldsymbol{z}) \#(15)$$

4 Experimental Results

In the experiment, the excitation signal is defined by

$$\boldsymbol{u_k} = \left[\boldsymbol{A_m}\ \mathbf{sin}\left(2\boldsymbol{\pi f k T_0} \right) + \boldsymbol{B} \right] \#(16)$$

Where, $\boldsymbol{A_m}$ and $\boldsymbol{B} = 0.4$. The excitation signal consists of a superposition of a DC component and a sinusoidal waveform, whose amplitude is restricted to a safe power range of 0-20 W. This configuration enables effective excitation of the system's low-frequency thermal dynamics while avoiding excessive heating that may cause tissue damage. The signal is applied to the microwave hyperthermia setup with a sampling period of $\boldsymbol{T_o}$ for model identification.

4.1 Linear Dynamic Model of Tissue Heating

In the experiment, a linear dynamic model is employed to approximate the microwave heating behavior, under the assumption that nonlinear factors, blood perfusion rate, and noise are negligible. This approximation is based on the premise that linear characteristics dominate the microwave heating mechanism, leading to the construction of the following linear dynamic model, i.e.

$$\hat{y}_k = -\hat{a}_1 \hat{y}_{k-1} - \hat{a}_2 \hat{y}_{k-2} + \hat{b}_0 u_{k-1} + \hat{c}_1 e_{k-1} \#(17)$$

where, $\hat{y}_k$ is the predicted output of the model. u is the input signal of the system. $\hat{a}_1$, $\hat{a}_2$, $\hat{b}_0$, $\hat{c}_1$ are the parameters that needs to be estimated. e_{k-1} is the prediction residual at time $k-1$. Subsequently, the RLS algorithm is applied for parameter identification, with the covariance matrix initialized as $P_k = 10^6 I_n$.

The fitting results presented in Figure 2 further confirm these limitations. Figure 3 depicts the residuals obtained using the RLS-based model. While the RLS-identified output generally captures the overall temperature trend, pronounced systematic oscillations are observed during the transient response. In particular, near the abrupt variation at approximately 120.6s, the RLS response exhibits a time delay of about 0.2s, failing to accurately track the rapid dynamics and leading to an instantaneous error greater than 0.3℃. This response delay reflects an intrinsic drawback of the RLS algorithm when handling fast time-varying dynamics, these results suggest that the identification process tends to converge to locally optimal solutions rather than the global optimum.

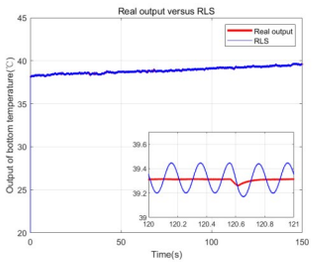

Figure 2 The curve obtained by fitting the RLS algorithm

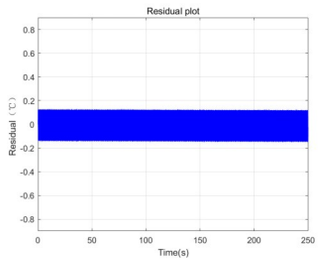

Figure 3 Model residuals identified by the RLS algorithm

To address these limitations, this study introduces an innovative hybrid identification framework that integrates the STOA with the FFRLS algorithm. By exploiting STOA's population-based intelligent search strategy, in which candidate solutions (sooty terns) cooperatively explore the parameter space using adaptive flight and spiral dive mechanisms, the framework achieves comprehensive global exploration, thereby effectively avoiding entrapment in local optima. The notable performance improvement stems from a dual-level optimization mechanism, in which the global search capability of STOA, facilitated by its dynamic step size and exploration-exploitation balancing strategy, ensures reliable parameter initialization, while the forgetting factor mechanism of FFRLS continuously tracks the system's slow time-varying characteristics, enabling refined parameter estimation throughout the identification process.

Figure 4 presents a comparative analysis of the identification results obtained by the RLS and STOA-FFRLS algorithms against the true system output, thereby providing further validation of the hybrid method's superior performance. Across the entire 150s experimental horizon, the STOA-FFRLS fitted curve maintains exceptional consistency with the measured temperature profile. At the critical abrupt change point t=120.6s, the response delay is reduced to less than 0.01s, while the instantaneous error drops to 0.15℃. Moreover, the maximum tracking error during the temperature-rising phase remains below 0.005℃.

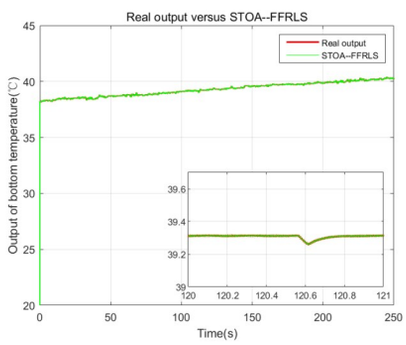

Figure 4 Model residuals identified by the STOA-FFRLS algorithm

STOA-FFRLS algorithm Residual analysis as shown in Figure 5 that the model's prediction error is strictly limited within the range of ±0.005℃, demonstrating its extremely high accuracy. In addition, the residuals show a consistent and continuous variation pattern. To quantify the performance improvement, Table 1 compares the mean squared error (MSE), mean absolute error (MAE), and root mean square error (RMSE) for model validation between the proposed STOA-FFRLS method and the conventional linear model, highlighting the improvement in performance. The results show that the MAE of the model identified using the RLS algorithm is 157 times higher than that of the STOA-FFRLS approach, while its MSE exceeds the latter by 4.986×10^5. These findings confirm that the proposed STOA-FFRLS algorithm achieves more accurate and stable modeling.

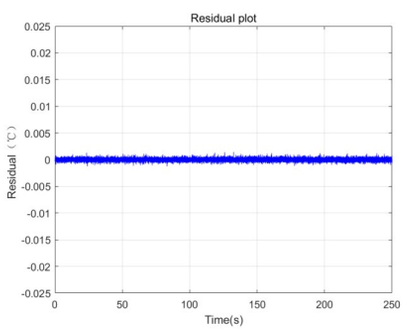

Figure 5 Model residuals identified by the STOA-FFRLS algorithm

Table 1 Model Validation Error Comparison

Modeling Method	MAE	MSE	RME
RLS	0.0795	0.008	0.0880
STOA-FFRLS	5.0600e-04	3.0954e-08	1.7594e-04

4.2 Linear Dynamic Conduction Model (LD-CM)

Considering the non-instantaneous dynamics between surface and underlying temperatures, and the fact that the actual bottom temperature cannot be directly observed, the model is formulated as

$$\hat{y}_k = -\hat{f}_1 \hat{x}_{k-1} + \hat{b}_1 u_{k-1} + \hat{b}_2 u_{k-2} \#(18)$$

where, $\hat{x}_{k-1}$ represents the bottom temperature estimated by the model at the previous step, $u $ is the surface temperature signal.

5 Conclusion

This study tackles the challenges of dynamic modeling for non-invasive temperature estimation in microwave hyperthermia systems by proposing a hybrid data-driven framework that combines the STOA with FFRLS. The STOA facilitates comprehensive global exploration of the parameter space through cooperative adaptive flight and spiral dive strategies, effectively mitigating the tendency of traditional recursive methods to become trapped in local optima. Concurrently, FFRLS ensures real-time adaptation and suppresses measurement noise via dynamic adjustment of the forgetting factor. Experimental results indicate that the proposed STOA-FFRLS framework achieves rapid convergence, high predictive accuracy, and robust performance, demonstrating its practicality and potential applicability in clinical thermal therapy.

References

[1] Nguyen PT, Abbosh A, Crozier S. Three-dimensional microwave hyperthermia for breast cancer treatment in a realistic environment using particle swarm optimization. IEEE Trans Biomed Eng. 2017; 64(6):1335-1344.

[2] Xi Z, et al. A preclinical system prototype and experimental validation of focused microwave brain hyperthermia. IEEE Trans Microw Theory Techn. 2025; 73(2):1147-1157.

[3] Amin B, et al. Dielectric characterisation of human adrenal glands and adrenal tumours for the development of microwave ablation technologies for hypertension treatment. Sci Rep. 2024; 14:19451.

[4] Duque J, Díaz I, Araque J. Thermal validation of a novel antenna design for superficial microwave hyperthermia. In: Proc IEEE 1st Latin Amer Conf Antennas Propag (LACAP). Cartagena de Indias, Colombia. 2024:1-2.

[5] Lestini F, DiCarlofelice A, Tognolatti P, Marrocco G, Occhiuzzi C. Experimental assessment of a smart skin for temperature monitoring during superficial microwave hyperthermia. IEEE J Electromagn RF Microw Med Biol. 2024.

[6] Ma M-L, et al. A non-invasive tumor hyperthermia method based on microwave field shaping. In: Proc Int Conf Microw Millim Wave Technol (ICMMT). Harbin, China. 2022:1-3.

[7] Duguet E. The effect of the incremental R&D tax credit on the private funding of R&D: an econometric evaluation on french firm level data [J]. Working Papers, 2012(03):405-435. Gonçalves MCT, Porter E, Conceição RC. Preliminary study of the mechanical properties of biological tissue during microwave hyperthermia. In: Proc 19th Eur Conf Antennas Propag (EuCAP). Stockholm, Sweden. 2025:1-5.

[8] Gaffoglio R, Giordanengo G, Righero M, Zucchi M, Firuzalizadeh M, et al. Real-time 3D temperature reconstruction in microwave cancer hyperthermia from scarce temperature measurements. Nat Commun. 2025;16(1):4824.

[9] Dhiman G, Kaur A. STOA: a bio-inspired optimization algorithm for industrial engineering problems. Engineering Applications of Artificial Intelligence. 2019;82:148-174.